molecular pharmaceutics

Article

Radioiodinated Portable Albumin Binder as a Versatile Agent for in vivo Imaging with Single-Photon Emission Computed Tomography

Xuejun Wen, Changrong Shi, Duo Xu, Pu Zhang, Zizhen Li, Jindian Li, Xinhui Su, Rongqiang Zhuang, Ting Liu, Zhide Guo, and Xianzhong Zhang

Mol. Pharmaceutics, **Just Accepted Manuscript** • DOI: 10.1021/acs.molpharmaceut.8b01116 • Publication Date (Web): 03 Jan 2019

Just Accepted

ACS Publications

is published by the American Chemical Society. 1155 Sixteenth Street N.W., Washington, DC 20036

Radioiodinated Portable Albumin Binder as a Versatile Agent for *in vivo* Imaging with Single-Photon Emission Computed Tomography

Xuejun Wen,[†] Changrong Shi,[†] Duo Xu,[†] Pu Zhang,[†] Zizhen Li,[‡] Jindian Li,[†] Xinhui Su,[#] Rongqiang Zhuang,[†] Ting Liu,[†] Zhide Guo,*[,†] Xianzhong Zhang*[,†]

[†] State Key Laboratory of Molecular Vaccinology and Molecular Diagnostics & Center for Molecular Imaging and Translational Medicine, School of Public Health, Xiamen University, 4221-116 Xiang'An South Rd, Xiamen 361102, China;

[‡] National Institute of Diagnostics and Vaccine Development in Infectious Diseases, Key Laboratory of the Ministry of Education for Cell Biology and Tumor Cell Engineering, School of Life Sciences, Xiamen University, Xiamen361102, China;

[#] ZhongshanHospital Affiliated to Xiamen University, Hubin South Road, Xiamen 361004, China.

ABSTRACT

In this study, radioiodinated 4-(p-iodophenyl)butyric acid ([^{131}I]IBA) was synthesized and evaluated as a portable albumin-binder for potential applications in SPECT imaging of blood pool, tumor and lymph node with significantly improved pharmacokinetic properties. The [^{131}I]IBA was prepared under the catalyst of Cu_2O/1,10-phenanthroline. After that, the albumin-binding capability of [^{131}I]IBA was tested *in vitro*, *ex vivo* and *in vivo*, respectively. [^{131}I]IBA was obtained with very high radiolabeling yield (> 99%) and good radiochemical purity (> 98%) within 10 min. It binds to albumin effectively with high affinity (IC_{50}= 46.5 μM) and has good stability. The results of biodistribution indicated that the [^{131}I]IBA was mainly accumulated in blood with good retention (10.51±2.58%ID/g at 30 min p.i. and 4.63±0.17%ID/g at 4 h p.i.). In the SPECT imaging of mice models with [^{131}I]IBA, blood pool, lymph node and tumors could be imaged clearly with high target-to-background ratio. Overall, the radioiodinated albumin binder of [^{131}I]IBA with long blood half-life and excellent stability could be used to decorate diversified albumin-binding radioligands and developed as a versatile theranostic agent.

Keywords: albumin binder, radioiodination, SPECT, animal models, in vivo imaging.

INTRODUCTION

The development of molecular imaging has provided renewed hope for disease diagnosis and therapy, which can offer the visualization, characterization, and measurement of biological processes at the molecular level.[1] During the design and synthetic phase, by improving *in vivo* pharmacokinetics of drugs, researchers move ever closer to the desired outcome. In general, getting the satisfactory target to non-target ratios within a relatively short time is an effective way of achieving a rapid diagnosis. While, in terms of traditional drugs, such as theranostic agents for cardiovascular diseases and tumor, short blood circulatory half-life fails to live up to their full potentials. Consequently, it is vital to research and develop effective drugs with optimal *in vivo* pharmacokinetics.[2] In such cases, just low dosages could achieve and maintain therapeutic effects, which reduce toxicity and the possibility of undesirable side effects.[3]

Albumin was regarded as a prominent carrier to protect drugs from enzymatic degradation and increase the half-lives.[4,5] We also anticipate that a wide range of biomedical applications for the albumin-binding moieties, particularly for the amelioration of pharmacokinetic properties. Previous literatures reported that truncated Evans Blue (EB) dye molecule could bind quantitatively to serum albumin *in vivo* and had been used for lymph node (LNs), tumor and blood pool imaging.[6,7] For example, ^{68}Ga ($t_{1/2}$=68 min) or ^{18}F labeled NEB has been used for PET imaging.[8,9]

Dumelin et al.[10] reported a class of albumin binders that displayed stable noncovalent binding interaction with human serum albumin (HSA). Among these binders, 4-(p-iodophenyl)butyricacid (4-IBA) was one of the promising structures, and has aroused great interest among the researchers in the molecular imaging field. Cristina Müller' team developed a series of DOTA/NOTA-folate conjugates containing the albumin-binding IBA entity to improve the tumor to kidney ratio as a consequence of a prolonged blood circulation time.[11-13] Likewise, some other agents, such as ^{177}Lu labeled prostate-specific membrane antigen (PSMA)-targeting ligands, also benefited from the albumin-binding motif.[14,15]

The goal of present work is to radioiodinate 4-IBA without destroying the

molecular structure and evaluate its potential application for SPECT imaging with long blood half-life and excellent *in vivo* stability. Compared with ^{99m}Tc or ^{18}F, both ^{125}I ($t_{1/2}$=60 d) and ^{131}I ($t_{1/2}$=8.03 d) have longer physical half-life, which have been widely used as therapeutic radionuclides to label albumin and other molecular structures.[16,17] Furthermore, the versatile characteristics of radioiodine isotopes (such as ^{123}I, ^{124}I, ^{125}I and ^{131}I) ensure the maximum satisfaction of theragnostic purposes. Therefore, radioiodinated 4-IBA was prepared using a convenient and quantitative radioiodination method via copper-mediated cross-coupling of aryl boronic acids.[18,19]

In addition to the amelioration of pharmacokinetic properties of different molecules, the radioiodinated IBA agent can be used for the examination and prediction of multiple diseases. In the present study, preliminary applications of radioiodinated IBA in the blood pool, tumor and lymphatic imaging with SPECT were performed.

EXPERIMENTAL SECTION

Reagents and Instruments

All chemicals were obtained commercially and used without further purification. The Na^{131}I were obtained from Zhongshan Hospital Affiliated to Xiamen University. The polyacetamide film was purchased from Pall Life Sciences and silica gel 60 F_{254} aluminum plates were purchased from Sinopharm Chemical Reagent Beijing Co., Ltd. The labeling efficiency and radiochemical purity were tested by Mini-Scan radio-TLC Scanner (BioScan, USA) and Dionex Ulti-Mate 3000 high-performance liquid chromatography (HPLC, Thermo Scientific, USA) with flow-counter radioactivity detector (BioScan, USA). The radioactivity was measured with γ-counter (WIZARD 2480, Perkin-Elmer, USA) and CRC-25R Dose Calibrator (CAPIN-TEC. Inc, USA). SPECT imaging was performed by using a nanoScan SPECT/CT scanner (Mediso, HUNGARY).

Animal Models

All the mice were obtained from the Laboratory Animal Center of Xiamen

University. Animal studies were approved by the national laws and carried out in compliance with the conduct of animal experimentation.

Inflamed LNs models: BALB/c mice were used to develop the hind limb LNs inflammation models. Mouse received a bilateral injection of 30 μL complete Freund adjuvant (Sigma Chemical) into the dorsal footpad, causing bilateral lymphadenitis. A few days later, SPECT imaging of inflamed LNs was performed. After imaging, EB dye was injected to identify lymphadenitis models.

4T1 murine breast tumor models: The right rear flanks of BALB/c mice were given a suspension of 4T1 murine breast cancer cells (5×10^6 cells of 4T1 in 50 μL PBS) subcutaneously. The mice were subjected to SPECT imaging when the tumor volume reached about 250 mm^3 (about 10 days after inoculation).

Orthotopic U87MG glioblastoma models: U87MG glioblastoma cells (1×10^5) stably transfected with a luciferase expression plasmid (U87MG-Luc) were suspended in sterile PBS, and stereotactically implanted in the right cerebral striatum of immunocompromised nude mice. Tumor growth was quantified weekly by bioluminescence imaging using a Xenogen In Vivo Imaging System after intraperitoneal injection of 110 mg/kg D-luciferin. The mice were subjected to SPECT imaging when the tumor volume reached about 100 mm^3.

Chemistry and Radiochemistry

The preparations of the desired compound [^{131}I]IBA and control compound 4-iodobenzoic acid ([^{131}I]IA) are shown in **Figure 1a** and **Figure S13a**.

Octanol/Water Partition Coefficient

To determine the hydrophilicity of [^{131}I]IBA, octanol/water partition coefficient (expressed as logP) was measured by using the reported method previously.[20,21] Briefly, 100 μL radiotracer solution was diluted with 2.9 mL PBS and 3 mL 1-octanol. After vortex blending for 3 min, the mixtures were centrifuged at 6000 rpm for 5 min. Then 100 μL organic layer was removed, and 2.9 mL 1-octanol and 3 mL PBS were added for another vortex blending and centrifugation. Repeat the process

and then the radioactive counts in the organic layer and inorganic layer (100 μL) were determined by γ-counter, respectively. The following equation was used to calculate P = (activity in octanol phase-background activity)/(activity in aqueous phase-background activity). All the experiments were performed with three independent measurements and reported as mean ±SD.

Interactions between [^{131}I]IBA and Proteins

The interaction of [^{131}I]IBA with albumin was tested using dialysis experiment. Dialysis membranes (molecular weight cut-off (MWCO) value of 7 kDa) containing radiolabeled compounds (about 18 MBq) and HSA (or BSA) were submerged in phosphate buffer (PB, pH 7.4) to remove the unbounded tracer. Radioactivity in PB and remained in membranes were measured by γ-counter and CRC-25R dose calibrator at different times, respectively. [^{131}I]IBA dialyzed against PB without HSA was performed for comparison. To explore the binding specificity, [^{131}I]IBA was added to the various type of proteins (HSA, hemoglobin and immunoglobulin) and incubated for 1 h at 37 °C. Then, the mixture was dialyzed in PB to remove the unbounded [^{131}I]IBA as described above. Furthermore, as a supplement, ultrafiltration was carried out to further validate the binding specificity. All experiments were performed with triplicate samples and reported as mean ± SD.

To learn more about the interaction between [^{131}I]IBA and protein, molecular docking technique was further employed to confirm binding site, binding force and energy of [^{131}I]IBA with HSA.

To determine whether the IBA and EB were in the same binding site, a competitive blocking experiment was performed. Briefly, [^{131}I]IBA and increasing concentrations of EB were incubated with albumin for 1 h at 37 °C. After incubation, an ultrafiltration membrane with an MWCO value of 10 kDa was used to separate unbounded [^{131}I]IBA. Thereafter, the radioactivity bound to HSA in ultrafiltration centrifuge was measured by γ-counter. Binding values were calculated by fitting the data with nonlinear regression using GraphPad Prism. Experiments were performed in triplicate.

In Vitro Binding Affinity Assays

In vitro albumin binding affinity of [^{131}I]IBA was measured via competition with nonradioactive IBA, by following the same steps as the above dialysis experiment. For comparison, EB was radioiodinated with ^{131}I using the iodogen method and the *in vitro* albumin binding affinity of [^{131}I]EB was measured as well (see **Supplementary Information**). Furthermore, the influences of precursor 4-(4-boronophenyl)butyric acid (4-BBA) on the albumin binding of [^{131}I]IBA were studied also. Briefly, [^{131}I]IBA (185 kBq) was incubated in albumin with the presence of increasing concentrations of 4-BBA for 1 h at 37 °C. After incubation, an ultrafiltration membrane with an MWCO value of 10 kDa was used to separate HSA bounded and unbounded [^{131}I]IBA. Thereafter, the radioactivity bound to HSA in ultrafiltration centrifuge was measured by γ-counter. The results were normalized in terms of the total added radioactivity (% of total activity). All the experiments were performed with triplicate samples and reported as mean ± SD.

Biodistribution Study

The biodistribution of [^{131}I]IBA was evaluated in normal and 4T1 tumor-bearing BALB/c mice (18-20 g, female), which were randomly divided into 7 and 4 groups (n=3), respectively. Approximately 370 kBq of the radiotracer (100 μL) was administered via a lateral tail vein of each mouse. Then the normal mice were sacrificed at 1 min, 30 min, 1 h, 2 h, 4 h, 12 h, and 24 h post-injection (p.i.) and the tumor-bearing mice were sacrificed at 2 h, 4 h, 6 h, and 12 h p.i. The interested tissues and organs were excised, weighed and counted by γ-counter. The results were calculated as a percentage of the injected dose per gram of tissues (%ID/g).

The biodistribution of [^{131}I]IA(370 kBq) in normal BALB/c mice was also performed at 1 min, 1 h, 4 h, 24 h p.i. (n=3/group) for comparison.

In Vivo SPECT/CT Imaging Study

About 7.4 MBq radiotracer (in 100 μL saline) was injected intravenously into each

4T1 tumor-bearing mouse and orthotopic U87MG model mouse, respectively, for SPECT/CT imaging studies using a nanoScanSPECT/CT preclinical scanner (Mediso, HUNGARY) at 15 min, 1 h, 2 h, 6 h, 24 h (4T1 tumor-bearing mice) or 2 h, 6 h, 12 h (U87MG glioblastoma models) p.i. The acquiring parameters were as follows: 364 keV energy peak for ^{131}I, window width of 20%, matrix of 256×256, medium zoom, and 48 frames (non-rotational acquisition of multipinhole SPECT for 30 s/frame). During acquisition, anesthesia was induced with 1.5% isoflurane to maintain spontaneous breathing of mice.

For SPECT imaging of lymphatic node, 0.74 MBq [^{131}I]IBA in 10 μL saline was injected into the footpad of each side of BALB/c mice. Then the mice were imaged at 30 min and 1 h p.i. with imaging parameters described above.

SPECT imaging of 4T1 tumor-bearing mice with [^{131}I]IA were conducted for comparison. About 7.4 MBq [^{131}I]IA (in 100 μL saline) was injected intravenously into each mouse and SPECT/CT images were acquired at 15 min, 2 h, 6 h and 24 h p.i.

Biological Safety

The toxicity of precursor 4-BBA and nonradioactive IBA were tested by MTT (methyl thiazolyl tetrazolium) experiments in 293T (human embryonic kidney cells) and LO2 cells (normal human hepatocyte). For the radiation safety, the medical internal radiation dose (MIRD) of [^{131}I]IBA was estimated based on biodistribution data by using OLINDA/EXM 1.1 code.

RESULTS

Chemistry and Radiochemistry

As shown in **Figure 1a**, [^{131}I]IBA-NHS was synthesized in the presence of Cu_2O and 1,10-phenanthroline according to a procedure reported by Zhang et al.[19] The 4-BBA and its active ester were characterized by ^{1}H-NMR and ^{13}C-NMR (**Figure S1** and **Figure S2**). The labeling progress of [^{131}I]IBA-NHS monitored by TLC was shown in **Figure S3**. The radioactive peak area of [^{131}I]IBA-NHS was exceeded 99%

within 10 min indicating high radiolabeling yield. As shown in **Figure S4-S7**, the radiochemical purity (>98%), specific activity (300 MBq/μmol) and stability were also determined by TLC and HPLC. The HPLC retention times of [^{131}I]IBA-NHS and [^{131}I]IBA were 5.23 and 4.16 min, respectively. [^{131}I]IBA was stable after incubated 24 h in saline or PB at different pH (from 4.5 to 8.5). The logP of [^{131}I]IBA was calculated as 1.01±0.03, indicating its moderate lipophilicity.

The protein-ligand interactions (including [^{131}I]IA and 4-BBA) were discussed in **Figure 1b**. Radioiodine labeled [^{131}I]EB was also obtained for comparison study, and its radiochemical purities (>99%) were confirmed by HPLC (**Figure S10**).

Interactions between [^{131}I]IBA and Proteins

As shown in **Figure S8a-c**, [^{131}I]IBA in dialysis bag without HSA was readily dialyzed into PB solution (88.46±1.28% of radioactivity at 24 h) and only 1.62±0.41% radioactivity remained in the bag after 24 h. In the presence of HSA, long-time radioactivity retention of [^{131}I]IBA in dialysis bag could be detected, indicating the effectively albumin-binding of [^{131}I]IBA. To further understand the binding specificity of [^{131}I]IBA, it was incubated with hemoglobin and immunoglobulin, respectively. The dialysis (**Figure S8d-f**) and filtered (**Figure S9a-b**) fraction of [^{131}I]IBA incubated with hemoglobin samples contained significant portions of radioactivity, indicating that most of the [^{131}I]IBA was bound to hemoglobin. While the [^{131}I]IBA-binding capacity of immunoglobulin was much weaker than that of HSA and hemoglobin. The binding specificity of [^{131}I]IBA was similar to [^{131}I]EB (**Figure S9c**).

According to the modeling results of HSA with IBA and IA (**Figure 2a**), the principal regions of intermolecular binding on HSA are located in hydrophobic cavities, which are corresponding to sites 1 and 2. The more detailed information of protein-ligand interaction was also evaluated by estimating energies of binding (shown in **Figure 2b)**. The binding energies between IBA and HSA were found to be -14.62 kcal/mol (site 1) and -16.75 kcal/mol (site 2), which indicated that the interaction between IBA and HSA was highly spontaneous and energetically

favorable. As a comparison, binding of IA-HSA was also studied by molecular docking, and the binding energy was found to be -7.38 kcal/mol (site 1) and -6.16 kcal/mol (site 2), which were higher than those of IBA-HSA. Moreover, as shown in **Figure 2c,** IBA and EB dye could bind HSA competitively, indicating the IBA and EB had similar binding sites.

In Vitro Binding Affinity Assays

In vitro albumin binding affinity of the [^{131}I]IBA was assessed via competition with different concentration of nonradioactive 4-IBA. As shown in **Figure S11a**, the [^{131}I]IBA showed eminent albumin-binding affinity with an IC_{50} value of 46.5 μM, which comparable to the radioiodinated EB ([^{131}I]EB, IC_{50} = 25.1 μM, **Figure S11b**). Furthermore, the result of ultrafiltration experiment (**Figure S12**) showed that the albumin-binding affinity of [^{131}I]IBA was basically impregnable in different concentration of 4-BBA.

Biodistribution Study

The biodistribution result of [^{131}I]IBA in normal mice was shown in **Figure 3a**. At 1 min p.i., much higher blood radioactivity (20.70±0.53%ID/g) was observed than the other tissues, indicating an initial accumulation in the circulation system. After 30 min injection, about half of the radioactivity uptake was cleared from blood and other major organs. The blood uptake was decreased to 10.51±2.58%ID/g, and the uptakes of the liver, kidney, lung were decreased from 5.47±0.38%ID/g, 8.83±1.40%ID/g, 11.18±4.76%ID/g to 2.93±0.11%ID/g, 4.47±0.13%ID/g, 5.68±0.40%ID/g, respectively. At 24 h p.i., the blood remained the highest accumulation (1.15±0.12%ID/g) when compared with the other tissues. As shown in **Table S1**, the ratios of blood to tissues were relatively high during the observation period indicating it might be a useful agent in blood pool imaging. Furthermore, the radioactivity in the thyroid was steadily low, confirming the good *in vivo* stability of the radiopharmaceuticals.

The biodistribution of [^{131}I]IBA in 4T1 tumor-bearing mice showed high tumor

uptake with good retention (**Table S2**). The sustained high tumor uptake (about 3%ID/g from 2 to 10 h p.i.) might due to the slow blood clearance of tracer. For the other organs, the biodistribution showed a similar trend with the results of normal mice.

[^{131}I]IA was selected as a control compound to validate the influence of molecular structure on the albumin binding ability. As illustrated in **Figure S13b**, the blood radioactivity was decreased to an extremely low level (0.57±0.08%ID/g) at 30 min p.i., the very fast blood clearance reflect very low albumin binding affinity of [^{131}I]IA when compared to [^{131}I]IBA (see the **Figure 3b and 3c**). This result confirmed that the efficient binding of [^{131}I]IBA to the proteins was due to the particular structure of 4-IBA.

***In Vivo* SPECT/CT Imaging Study**

In vivo SPECT/CT scans of 4T1 tumor mice were shown in **Figure 4a**. After i.v. injection of [^{131}I]IBA, long lasting high radioactivity accumulation in the heart and blood vessels allowed the visualization of radioactive distribution with SPECT. At the same time, increased tumor uptake of [^{131}I]IBA was observed at later time points. The low uptakes in the background and non-target organs leading to high SPECT image contrast. Furthermore, the negligible thyroid radioactivity reaffirmed the good *in vivo* stability of [^{131}I]IBA. After SPECT imaging, the tumor region was further identified by *in vivo* MRI imaging and *in vitro* haematoxylin and eosin (H&E) staining to discriminate the necrosis part from the active tumor area (**Figure 4b and 4c**). As shown in **Figure 4d**, there was no obvious difference between the tumor and surrounding muscle at 15 min p.i., while the T/NT ratios (tumor/liver and tumor/muscle ratios were increased obviously at later time points (from 1.65 and 3.35 to 2.76 and 3.87 from 1 h to 6 h p.i.). The enhanced tumor uptake might due to the slow blood clearance of [^{131}I]IBA. These imaging results are in accordance well with that of biodistribution. The fast blood clearance and negligible tumor radioactivity of control agent [^{131}I]IA (**Figure S13c**) further demonstrated the low albumin binding affinity of 4-iodobenzoic acid.

The successful imaging of subcutaneous tumor motivated us to further explore more complex applications, especially for an orthotropic brain tumor and inflamed LNs models. For SPECT imaging of brain tumor (**Figure 5a**), due to the low level of radioactivity in the normal brain and high uptake in tumor regions, these circumstances resulted in a high tumor-to-brain ratio. The ratio of tumor-to-brain reached to 5.75±0.32 at 12 h p.i. (**Figure 5b**). As shown in **Figure 5c**, the orthotopically implanted Luc-expressing U87MG glioma tumor models were further verified by bioluminescence 750 imaging.

To verify the potential of [^{131}I]IBA for LNs imaging, inflamed LNs models were established. The hotspot was displayed through maximum intensity projection (MIP). Fusion of SPECT/CT images confirmed the anatomic location of the popliteal LNs. As shown in **Figure 6,** inflamed popliteal LNs on both sides were clearly seen on SPECT images, with a high signal to background ratio at all time points examined. Based on the analysis of these images, we found that LNs in different states had obviously different tracer uptakes. To understand the sources of this difference, after imaging, EB dye was injected into soles to identify lymphadenitis models (**Figure 6a(ii), b(ii) and c(ii)**). The LNs with the significant signal intensity of dye matched exactly with the hotspots in SPECT images. The mouse was sacrificed after SPECT imaging, and the bilateral LNs were dissected and observed. Through the anatomical analysis in **Figure 6b(ii) and 6c(ii)**, it was found that the left popliteal LNs were enlarged due to the inflammatory stimulation, which was consistent with the messages in **Figure 6b(i) and 6c(i)**. Quantification of the SPECT images showed that uptake of [^{131}I]IBA in the inflamed LN was 0.21%ID, which was significantly higher than that in the contralateral LN (0.02%ID) at 1 h p.i. (**Figure 6b**). Along with the inflammation development, the activity-rich region was expanded (**Figure 6c**).

Biological Safety

MTT assay of precursor 4-BBA and nonradioactive IBA at various concentrations in 293T and LO2 cells was tested. The results showed that 4-BBA and IBA had little effect on cell viability at concentrations below 0.1 mg/mL (**Figure S14**). To estimate

the safe dosage for clinical use, total absorbed radiation dosage based on biodistribution data was estimated by OLINDA/EXM software (as shown in **Table S3**). The administration of [^{131}I]IBA was well tolerated, with no marked effects on vital signs. This dosage provided a more accurate estimate of the dosimetry clinically for human scans in the future.

DISCUSSION

As we all know, there are several agents for the circulation system or tumor imaging have been explored and developed. The ^{99m}Tc ($t_{1/2}$=6.02 h) labeled red blood cells (^{99m}Tc-RBCs) as the major imaging agent for radionuclide angiography, had been used clinically as early as 1958 for determining total blood and plasma volume.[22,23] ^{99m}Tc-Sulfurcolloid (^{99m}Tc-SC) has long been used in the imaging of LNs. However, it is plagued by slow transport from the injection site.[24] It is also a pity that, in the cases of radionuclide therapy, these radiotracers are powerless. Relatively, radioiodine isotopes are clearly the more versatile and favorable radionuclides. Radioiodinated albumin can be used as a blood pool imaging agent to determine the circulating plasma volume, amount of blood circulation and blood circulation time, etc.[25] Unfortunately, the common methods of radiolabeling albumin *in vitro* (such as chloramine-T method for radioiodine labeling) come with many disadvantages like the instability of product, protein degeneration, product contamination and immunological rejection reaction. The unfavorable pharmacokinetics of these tracers could be crucial factors degrading the quality of imaging. Among the *in vivo* and *in vitro* albumin-labeled molecules, EB dye is a representative one. However, the preparation of EB derivatives requires harsh conditions and tedious procedures.[6] Moreover, EB molecule can't be labeled with radionuclides (^{18}F, ^{68}Ga or ^{177}Lu) directly, chemical modification with bifunctional chelators such as NOTA or DOTA is needed to chelate diagnostic or therapeutic radionuclides, which add new complexities.[9,26,27]

Based on the results of previous literature,[10] we develop the *in vivo* albumin-labeling method to meet the needs for both preclinical evaluation and clinical

application. The preparation procedure of radioiodinated 4-IBA is rapid, efficient and simple, which has great potential for clinical translation. As mentioned above, nonradioactive IBA has been utilized as an albumin binding molecule to modulate pharmacokinetics for therapeutic purposes. [^{131}I]IBA, compared with EB dyes, has several eminent advantages: mild labeling conditions, simple operational processes and stable chemical structure, no obvious deiodination is observed *in vivo* and *in vitro* experiments, which is agreed well with the previous studies.[18,19,28] In contrast, as shown in **Figure S15**, [^{131}I]EB has shortage instability, which degenerates the images seriously. Tedious purification processes were always bottlenecks restricting the next application of drug candidates. And at the same time, radioactivity loss during purification processes was not to be ignored. The facile radioiodination of aromatic and heteroaromaticboronic acid systems provided ultra-high labeling yield and excellent radiochemical yield. Furthermore, after radiolabeling, superfluous precursor boronic acid substrate had no impact on the albumin-binding affinity of the aimed product, which meant further purification was unnecessary (see **Figure 1b** and **Figure S12**). And more importantly, the radioiodinated portable IBA-NHS can serve as a "Bolton-Hunter" reagent or a versatile intermediate, which could be conveniently converted into the desired targeting or therapeutic molecules through the simplest chemical reaction at RT, without requiring extra functional chelating agents. Stability properties and long half-life provide a foundation for transport transfer.

In the present work, the potential application of [^{131}I]IBA were demonstrated in the blood pool, tumor and LNs imaging. High radioactivity retained in the blood circulatory system after i.v. injection verify the feasibility of using the tracer as a blood-pool imaging agent. More importantly, the high accumulation of [^{131}I]IBA in the tumor is afforded by albumin binding and resulted in enhanced imaging contrast. As shown in **Figure 4**, this agent could also be used to distinguish tumor and necrosis sites, detect tumor activity and monitor the progress of tumor. And as expected, the *in vivo* labeling strategy can also be applied to evaluate the lymphatic system under both physiologic and pathologic circumstances (such as inflamed LNs). Better yet, these encouraging results are not mediated and affected by receptors expressed in cancer

cells. By contrast, the albumin binding affinity of [^{131}I]EB has a narrow lead over that of [^{131}I]IBA (IC_{50}: 25.1 μM vs. 46.5 μM). Whereas, relatively high thyroid and stomach uptakes were achieved because [^{131}I]EB is unstable *in vivo*. From these results, we can see that radioiodinated IBA is comparable to radiolabeled EB tracers for tumors and LNs imaging.[10,24,29] Thus, radioiodinated IBA is a capable albumin-binding radiotracer like EB agents, which has been successfully demonstrated in the modification of several radiolabeled targeting molecules (RGD [3], PMSA [14], Octreotide [30], Exendin-4 [31], etc.). In some ways, IBA provides even more extensive features.

CONCLUSIONS

A novel radioiodinated portable albumin binding moiety was obtained with high-efficiency synthesis processes and mild reaction conditions. Our study indicated that this moiety has long blood half-life and good stability, which is well-tolerated with regard to the interactions of the compound with serum proteins. Hence, the radioiodinated IBA has great potential for clinical application in the blood pool, tumors and LNs imaging. In addition, this radioiodinated albumin binder is transferable to other molecules or targeting agents to facilitate the design of albumin-binding radioligands and perfect their pharmacokinetics. This will be the main contents in future research.

ASSOCIATED CONTENT

Supporting Information

The details of chemical synthesis routes, characterization of compounds and biodistribution were described in the supplementary file. This material is available free of charge via the Internet at http://pubs.acs.org.

AUTHOR INFORMATION

*Corresponding authors

Xianzhong Zhang (Ph.D., Professor) and Zhide Guo (Ph.D.). Center for Molecular Imaging and Translational Medicine, School of Public Health, Xiamen University, 4221-116 Xiang'An South Rd, Xiamen 361102, China. E-mail: zhangxzh@xmu.edu.cn; gzd666888@xmu.edu.cn.

Author contributions

Xianzhong Zhang, Zhide Guo and Xuejun Wen were responsible for the conception and design of the study, the acquisition and analysis of the data, the drafting of the manuscript, and final approval of the version to be published. Ting Liu and Rongqiang Zhuang contributed to critical revision for important intellectual content, and final approval of the version to be published. Changrong Shi, Duo Xu, Pu Zhang, Zizhen Li and Jindian Li contributed to acquisition, analysis and interpretation of data. Xinhui Su contributed to critical revision of the manuscript for important intellectual content and material support.

Notes

The authors declare no competing financial interest.

Acknowledgments

This study was financially supported by the National Natural Science Foundation of China (81471707), Postdoctoral Science Foundation of China (2018M630732), China Postdoc Innovation Talent Supporting Program (BX201700142) and Science

1 Foundation of the Fujian Province, China (Grant No. 2016J05200).

ABBREVIATIONS

The following abbreviations are used in this manuscript:

IBA, 4-(p-iodophenyl)butyric acid

4-BBA, 4-(4-boronophenyl)butyric acid

IA, 4-iodobenzoic acid

EB, Evans Blue

LNs, lymph nodes

HSA, human serum albumin

PSMA, prostate-specific membrane antigen

MWCO, molecular weight cut-off

MTT, methyl thiazolyl tetrazolium

MIRD, medical internal radiation dose

H&E, haematoxylin and eosin staining

SPECT, single photon emission computed tomography

PET, positron emission tomography

MRI, magnetic resonance imaging

PB, phosphate buffer

%ID/g, percentage of injected dose per gram

ROIs, regions of interests

T/NT, tumor-to-non-target-tissue

MIP, maximum intensity projection

HPLC, High Performance Liquid Chromatography

RBCs, red blood cells

^{99m}Tc-SC, ^{99m}Tc-Sulfurcolloid

DOTA, 1,4,7,10-Tetraazacyclododecane-1,4,7,10-tetraacetic acid

NOTA, 1,4,7-triazacyclononane-1,4,7-triacetic acid

REFERENCES

(1) Liang, G.; Nguyen, P. K., Molecular probes for cardiovascular imaging. *J. Nucl. Cardiol.* **2016,** 23, 783-789.

(2) Dennis, M. S.; Zhang, M.; Meng, Y. G.; Kadkhodayan, M.; Kirchhofer, D.; Combs, D.; Damico, L. A., Albumin binding as a general strategy for improving the pharmacokinetics of proteins. *J. Biol. Chem.* **2002,** 277, 35035-35043.

(3) Chen, H.; Jacobson, O.; Niu, G.; Weiss, I. D.; Kiesewetter, D. O.; Liu, Y.; Ma, Y.; Wu, H.; Chen, X., Novel "add-on" molecule based on Evans Blue confers superior pharmacokinetics and transforms drugs to theranostic agents. *J. Nucl. Med.* **2017,** 58, 590-597.

(4) Chuang, V. T.; Kragh-Hansen, U.; Otagiri, M., Pharmaceutical strategies utilizing recombinant human serum albumin. *Pharm. Res.* **2002,** 19, 569-577.

(5) Basuli, F.; Li, C.; Xu, B.; Williams, M.; Wong, K.; Coble, V. L.; Vasalatiy, O.; Seidel, J.; Green, M. V.; Griffiths, G. L., Synthesis of fluorine-18 radio-labeled serum albumins for PET blood pool imaging. *Nucl. Med. Biol.* **2015**, 42, 219-225.

(6) Niu, G.; Chen X., Lymphatic imaging: focus on imaging probes. *Theranostics.* **2015,** 5, 686-697.

(7) Jacobson, O.; Kiesewetter, D. O.; Chen, X., Albumin-binding Evans Blue derivatives for diagnostic imaging and production of long-acting therapeutics. *Bioconjug. Chem.* **2016,** 27, 2239-2247.

(8) Zhang, W.; Wu, P.; Li, F.; Tong, G.; Chen, X.; Zhu, Z., Potential applications of using ^{68}Ga-Evans Blue PET/CT in the evaluation of lymphatic disorder preliminary observations. *Clin. Nucl. Med.* **2016,** 41, 302-308.

(9) Zhang, J.; Lang, L.; Zhu, Z.; Li, F.; Niu, G.; Chen, X., Clinical translation of an albumin-binding PET radiotracer Ga-68-NEB. *J. Nucl. Med.* **2015,** 56, 1609-1614.

(10) Dumelin, C. E.; Trussel, S.; Buller, F.; Trachsel, E.; Bootz, F.; Zhang, Y.; Mannocci, L.; Beck, S. C., Drumea-Mirancea, M., Seeliger, M. W., A portable albumin binder from a DNA-encoded chemical library. *Angew. Chem. Int. Edit.* **2008,** 47, 3196-3201.

(11) Siwowska, K.; Haller, S.; Bortoli, F.; Benešová, M.; Groehn, V.; Bernhardt, P.; Schibli, R.; Müller, C., Preclinical comparison of albumin-binding radiofolates: impact of linker entities on the *in vitro* and *in vivo* properties. *Mol. Pharmaceut.* **2017,** 14, 523-532.

(12) Farkas, R.; Siwowska, K.; Ametamey, S. M.; Schibli, R.; van der Meulen, N. P.; Müller, C., ^{64}Cu- and ^{68}Ga-based PET imaging of folate receptor-positive tumors: development and evaluation of an

albumin-binding NODAGA-folate. *Mol. Pharmaceut.* **2016,** 13, 1979-1987.

(13) Müller, C.; Struthers, H.; Winiger, C.; Zhernosekov, K.; Schibli, R., DOTA conjugate with an albumin-binding entity enables the first folic acid-targeted ^{177}Lu-radionuclide tumor therapy in mice. *J. Nucl. Med.* **2013,** 54, 124-131.

(14) Choy, C. J.; Ling, X.; Geruntho, J. J.; Beyer, S.K.; Latoche, J. D.; Langton-Webster, B.; Anderson, C. J.; Berkman, C. E., ^{177}Lu-labeled phosphoramidate-based PSMA inhibitors: the effect of an albumin binder on biodistribution and therapeutic efficacy in prostate tumor-bearing mice. *Theranostics.* **2017,** 7, 1928-1939.

(15) Umbricht, C. A.; Benesova, M.; Schibli, R.; Müller, C., Preclinical development of novel PSMA-targeting radioligands: modulation of albumin-binding properties to improve prostate cancer therapy. *Mol. Pharmaceut.* **2018,** 15, 2297-2306.

(16) Cavina, L.; van der Born, D.; Klaren, P. H. M.; Feiters, M. C.; Boerman, O. C.; Rutjes, F. P. J. T., Design of radioiodinated pharmaceuticals: structural features affecting metabolic stability towards *in vivo*deiodination. *Eur. J. Org. Chem.* **2017,** 24, 3387-3414.

(17) Kojima, A.; Gotoh, K.; Shimamoto, M.; Hasegawa, K.; Okada, S., Iodine-131 imaging using 284 keV photons with a small animal CZT-SPECT system dedicated to low-medium-energy photon detection. *Ann. Nucl. Med.* **2016,** 30, 169-175.

(18) Zhang, P.; Zhuang, R.; Wang, X.; Liu, H.; Li, J.; Su, X.; Chen, X.; Zhang, X., Highly Efficient and Stable Strain-Release Radioiodination for Thiol Chemoselective Bioconjugation. *Bioconjug. Chem.* **2018,** 29, 467-472.

(19) Zhang, P.; Zhuang, R.; Guo, Z.; Su, X.; Chen, X.; Zhang, X., A highly efficient copper-mediated radioiodination approach using aryl boronic acids. *Chem-Eur. J.* **2016,** 22, 16782-16785.

(20) Guo, Z.; Zhang, P.; Song, M.; Wu, X.; Liu, C.; Zhao, Z.; Lu, J.; Zhang, X., Synthesis and preliminary evaluation of novel Tc-99m-labeled folate derivative via click reaction for SPECT imaging. *Appl. Radiat. Isot.* **2014,** 91, 24-30.

(21) Guo, Z.; Gao, M.; Song, M.; Shi, C.; Zhang, P.; Xu, D.; You, L.; Zhuang, R.; Su, X.; Liu, T., Synthesis and evaluation of Tc-99m-labeled dimeric folic acid for FR-targeting. *Molecules.* **2016,** 21, 817-829.

(22) Stedrova, V.; Laub, T.; Koudelova, M., Localization and confirmation of splenosis by SPECT/low dose CT with ^{99m}Tc labelled hot-damaged red blood cells-2 case report. *Eur. J. Nucl. Med. Mol.*

Imaging. **2010,** 37, S495-S495.

(23) Lambert, B.; Mertens, J.; Sturm, E. J.; Stienaers, S.; Defreyne, L.; D'Asseler, Y., Tc-99m-labelled macroaggregated albumin (MAA) scintigraphy for planning treatment with Y-90 microspheres. *Eur. J. Nucl. Med. Mol. Imaging.* **2010,** 37, 2328-2333.

(24) Wang, Y.; Lang, L.; Huang, P.; Wang, Z.; Jacobson, O.; Kiesewetter, D. O.; Ali, I. U.; Teng, G.; Niu, G.; Chen, X., *In vivo* albumin labeling and lymphatic imaging. *Proc. Natl. Acad. Sci. USA.* **2015,** 112, 208-213.

(25) Mozaffarian, D.; Benjamin, E. J.; Go, A. S.; Arnett, D. K.; Blaha, M. J.; Cushman, M.; Das, S. R.; de Ferranti, S.; Després, J. P.; Fullerton, H. J., Heart disease and stroke statistics-2016 update: a report from the American heart association. *Circulation.* **2016,** 133, E38-E360.

(26) McBride, W. J.; D'Souza, C. A.; Sharkey, R. M.; Karacay, H.; Rossi, E. A.; Chang, C. H.; Goldenberg, D. M., Improved F-18 labeling of peptides with a fluoride-aluminum-chelate complex. *Bioconjug. Chem.* **2010,** 21, 1331-1340.

(27) Bandara, N.; Jacobson, O.; Mpoy, C.; Chen, X.; Rogers, B. E., Novel Structural Modification Based on Evans Blue Dye to Improve Pharmacokinetics of a Somastostatin-Receptor-Based Theranostic Agent. *Bioconjug. Chem.* **2018,** 29, 2448-2454.

(28) Tang, L.; Peng, C.; Tang, B.; Li, Z.; Wang, X.; Li, J.; Gao, F.; Huang, L.; Xu, D.; Zhang, P., Radioiodinated Small Molecule Tyrosine Kinase Inhibitor for HER2 Selective SPECT Imaging. *J. Nucl. Med.* **2018,** 59, 1386-1391.

(29) Niu, G.; Lang, L.; Kiesewetter, D. O.; Ma, Y.; Sun, Z.; Guo, N.; Guo, J.; Wu, C.; Chen, X., *In vivo* labeling of serum albumin for PET. *J. Nucl. Med.* **2014,** 55, 1150-1156.

(30) Zhang, J.; Wang, H.; Jacobson, O.; Cheng, Y,; Niu, G.; Li, F.; Bai, C.; Zhu, Z.; Chen, X., Safety, Pharmacokinetics, and Dosimetry of a Long-Acting Radiolabeled Somatostatin Analog ^{177}Lu-DOTA-EB-TATE in Patients with Advanced Metastatic Neuroendocrine Tumors. *J. Nucl. Med.* **2018,** 59, 1699-1705.

(31) Chen, H.; Wang, G.; Lang, L.; Jacobson, O.; Kiesewetter, D.O.; Liu, Y.; Ma, Y.; Zhang, X.; Wu, H.; Zhu, L.; Niu, G.; Chen, X., Chemical Conjugation of Evans Blue Derivative: A Strategy to Develop Long-Acting Therapeutics through Albumin Binding. *Theranostics*. **2016,** 6, 243-253.

The legends of tables and figures:

Figure 1. (a) Chemical synthesis route and radiolabeling process of [^{131}I]IBA. (b) Illustration for the protein-ligand interactions.

Figure 2. (a) Docking of IBA and IA to HSA. (b) The binding energy of probes and HSA. (c) The albumin binding ratios of IBA were obtained in the presence of different EB dye concentrations.

Figure 3. (a) The biodistribution results of [^{131}I]IBA in normal mice (%ID/g, mean±SD, n=3). (b) Blood elimination curve of [^{131}I]IBA and [^{131}I]IA. (c) The percentage curve of blood elimination rate of [^{131}I]IBA and [^{131}I]IA.

Figure 4. (a) MIP SPECT/CT images of 4T1 tumor mice after intravenous injection of 7.4 MBq [^{131}I]IBA. (b) After SPECT imaging, the tumor region was further identified by MRI. (c) H&E staining was used to discriminate necrosis and tumor. (d) T/NT ratios at different time-points. Data are shown as mean ± SD (n=3).

Figure 5. (a) SPECT/CT images of brain tumor mice after intravenous injection of 7.4 MBq [^{131}I]IBA (2 h, 6 h and 12 h p.i.). (b) Tumor/brain ratios at different time-points. Data are shown as mean ± SD (n=3). (c) The tumor region was further identified by bioluminescence imaging.

Figure 6. (a(i), b(i), c(i)) MIP SPECT/CT images of inflamed LNs models at different stages. The inflamed popliteal LNs were indicated by red arrows. Quantitative analysis of [^{131}I]IBA uptake in LNs was calculated as a percentage of the injected dose. (a(ii), b(ii), c(ii)) LNs mapping with EB dye in inflamed LNs models. Red arrows indicate popliteal LNs with blue color, and black arrowheads indicate the injection site.

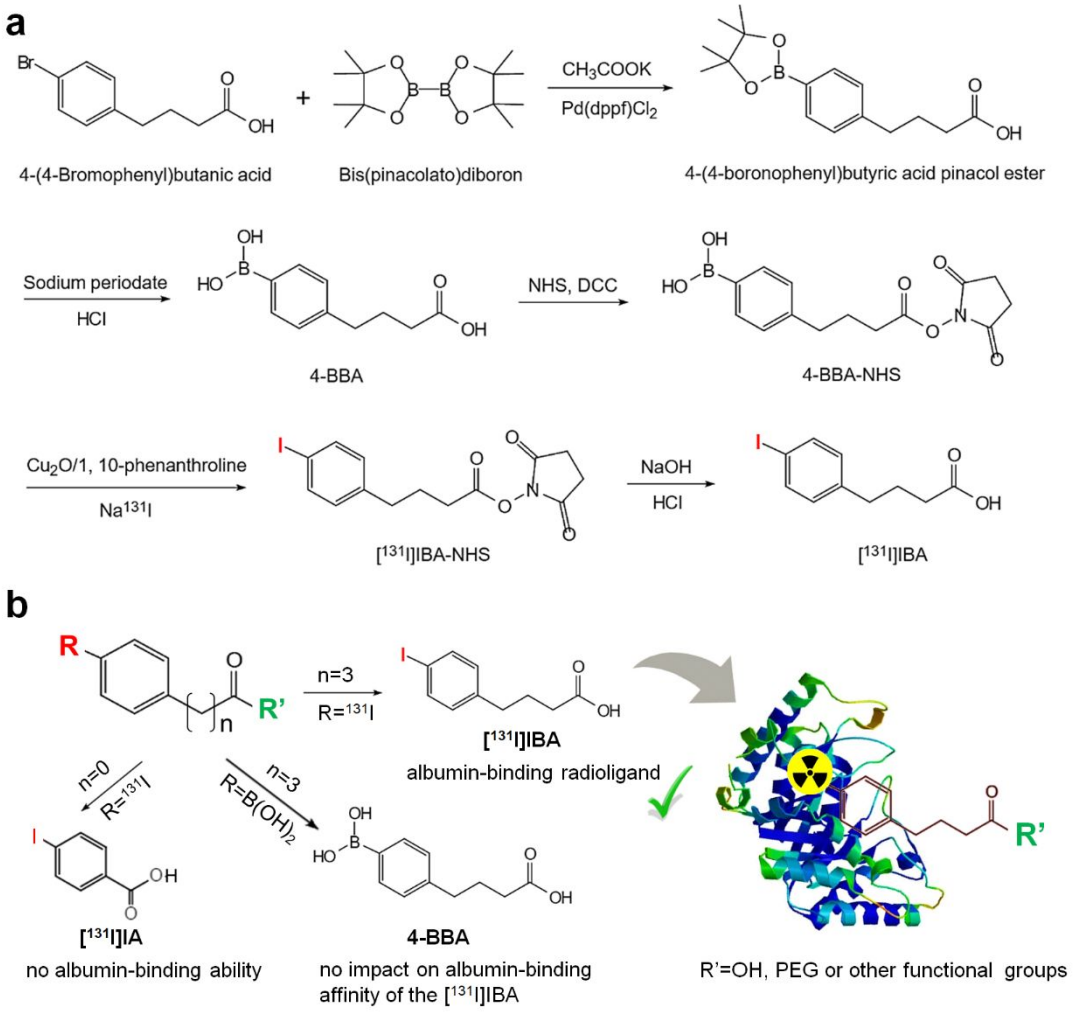

Figure 1. (a) Chemical synthesis route and radiolabeling process of [^{131}I]IBA. (b) Illustration for the protein-ligand interactions.

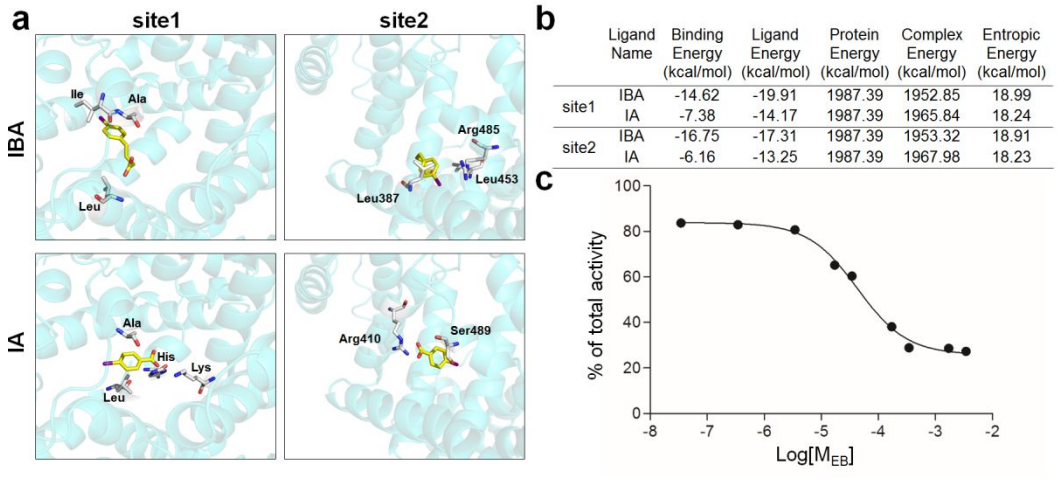

	Ligand Name	Binding Energy (kcal/mol)	Ligand Energy (kcal/mol)	Protein Energy (kcal/mol)	Complex Energy (kcal/mol)	Entropic Energy (kcal/mol)
site1	IBA	-14.62	-19.91	1987.39	1952.85	18.99
	IA	-7.38	-14.17	1987.39	1965.84	18.24
site2	IBA	-16.75	-17.31	1987.39	1953.32	18.91
	IA	-6.16	-13.25	1987.39	1967.98	18.23

Figure 2. (a) Docking of IBA and IA to HSA. (b) The binding energy of probes and HSA. (c) The albumin binding ratios of IBA were obtained in the presence of different EB dye concentrations.

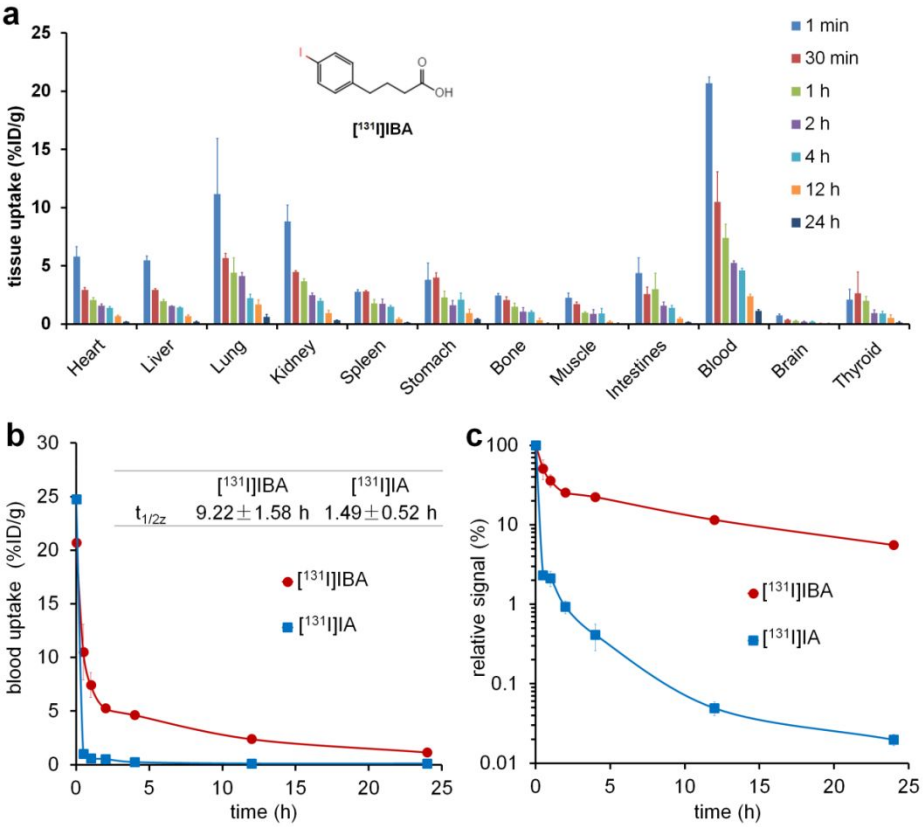

Figure 3. (a) The biodistribution results of [^{131}I]IBA in normal mice (%ID/g, mean±SD, n=3). (b) Blood elimination curve of [^{131}I]IBA and [^{131}I]IA. (c) The percentage curve of blood elimination rate of [^{131}I]IBA and [^{131}I]IA.

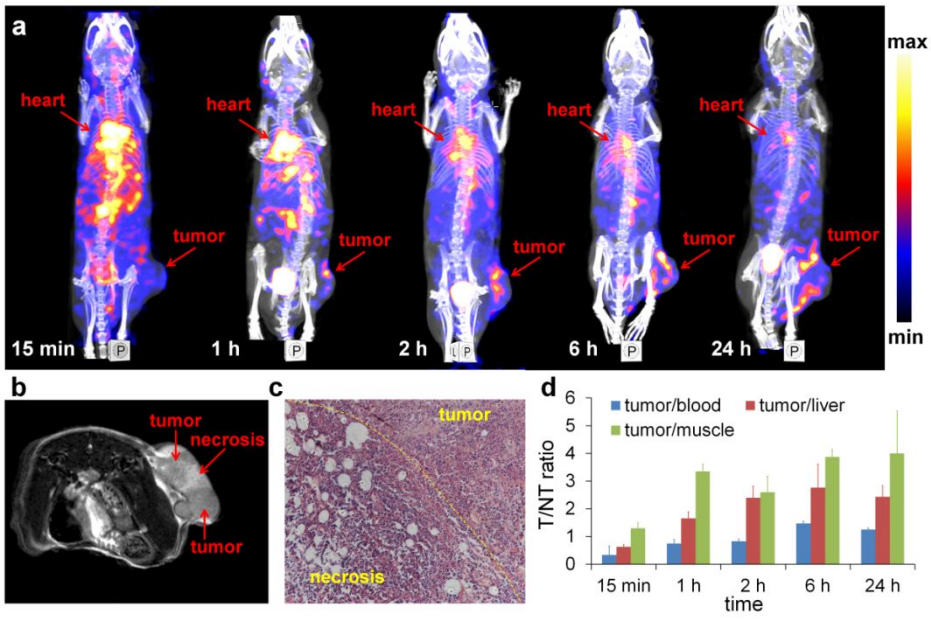

Figure 4. (a) MIP SPECT/CT images of 4T1 tumor mice after intravenous injection of 7.4 MBq [^{131}I]IBA. (b) After SPECT imaging, the tumor region was further identified by MRI. (c) H&E staining was used to discriminate necrosis and tumor. (d) T/NT ratios at different time-points. Data are shown as mean ± SD (n=3).

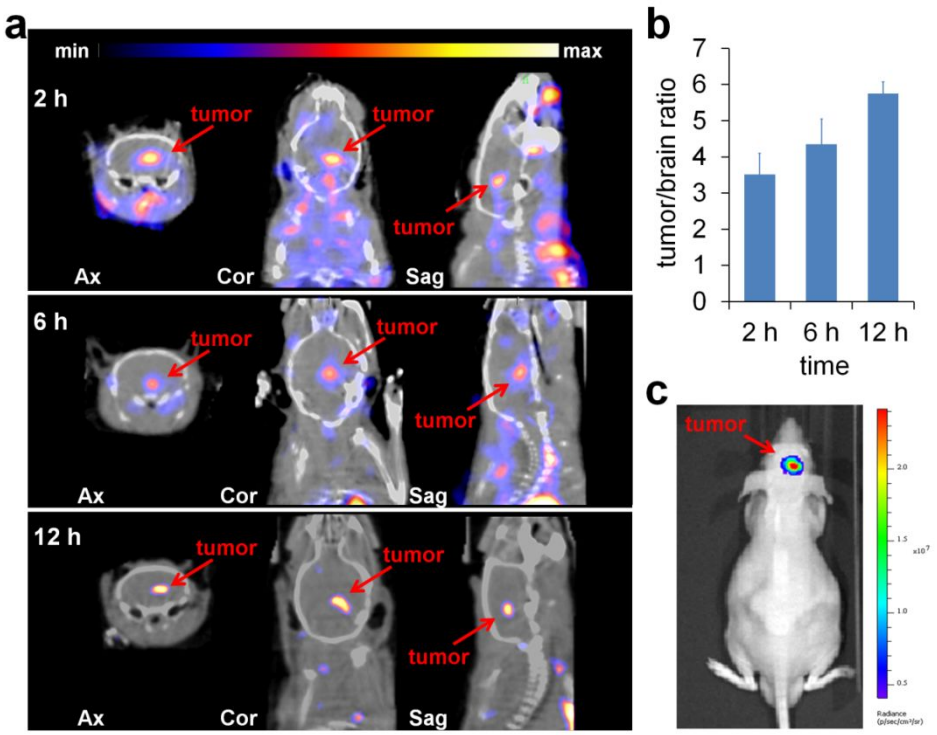

Figure 5. (a) SPECT/CT images of brain tumor mice after intravenous injection of 7.4 MBq [^{131}I]IBA (2 h, 6 h and 12 h p.i.). (b) Tumor/brain ratios at different time-points. Data are shown as mean ± SD (n=3). (c) The tumor region was further identified by bioluminescence imaging.

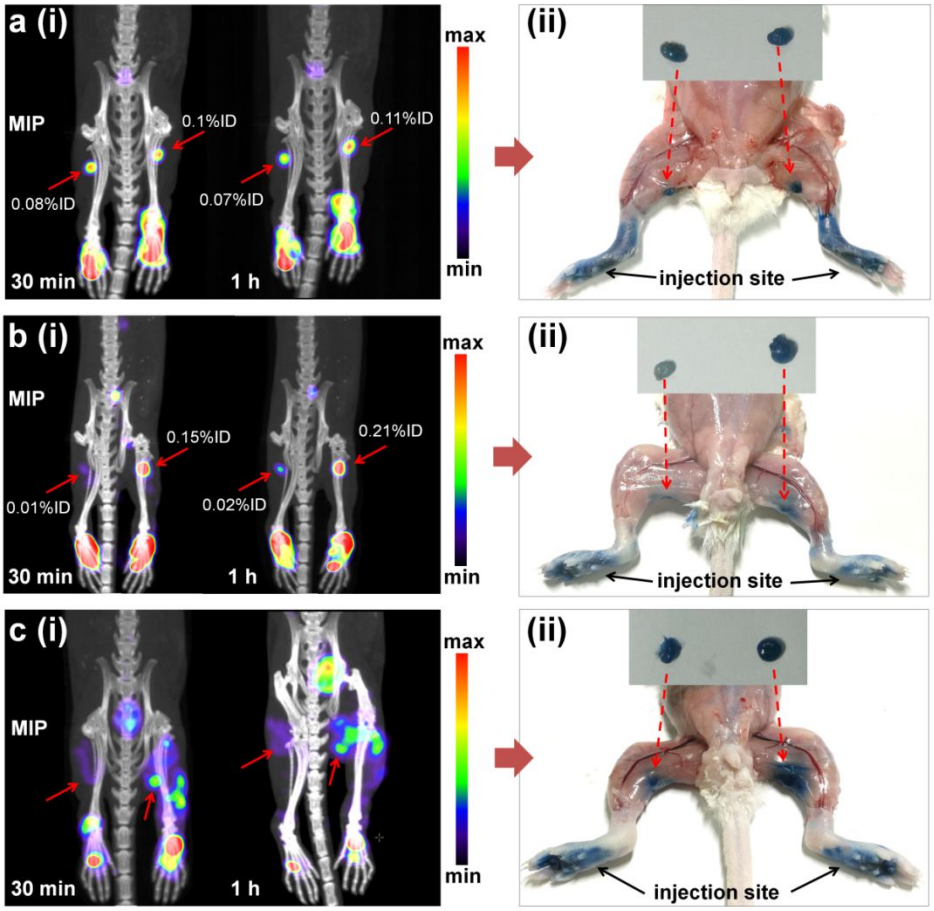

Figure 6. (a(i), b(i), c(i)) MIP SPECT/CT images of inflamed LNs models at different stages. The inflamed popliteal LNs were indicated by red arrows. Quantitative analysis of [^{131}I]IBA uptake in LNs was calculated as a percentage of the injected dose. (a(ii), b(ii), c(ii)) LNs mapping with EB dye in inflamed LNs models. Red arrows indicate popliteal LNs with blue color, and black arrowheads indicate the injection site.

Table of Contents